PASJ: Publ. Astron. Soc. Japan **59**, S649–S654, 2007 November 30

Small-Scale Magnetic-Flux Emergence Observed with Hinode Solar Optical Telescope

Kenichi OTSUJI,[1,2] Kazunari SHIBATA,[2] Reizaburo KITAI,[2] Satoru UENO,[2] Shin'ichi NAGATA,[2] Takuma MATSUMOTO,[1,2] Tahei NAKAMURA,[1,2] Hiroko WATANABE,[1,2] Saku TSUNETA,[3] Yoshinori SUEMATSU,[3] Kiyoshi ICHIMOTO,[3] Toshifumi SHIMIZU,[4] Yukio KATSUKAWA,[3] Theodore D. TARBELL,[5] Bruce LITES,[6] Richard A. SHINE,[5] and Alan M. TITLE[5]

[1]*Department of Astronomy, Kyoto University, Kitashirakawa-Oiwake-cho, Sakyo-ku, Kyoto 606-8502*
otsuji@kwasan.kyoto-u.ac.jp
[2]*Kwasan and Hida Observatories, Kyoto University, Yamashina-ku, Kyoto 607-8471*
[3]*National Astronomical Observatory of Japan, 2-21-1 Osawa, Mitaka, Tokyo 181-8588*
[4]*Institute of Space and Astronautical Science, Japan Aerospace Exploration Agency, 3-1-1 Yoshinodai, Sagamihara, Kanagawa 229-8510*
[5]*Lockheed Martin Solar and Astrophysics Laboratory, 3251 Hanover Street, Palo Alto, CA 94304, USA*
[6]*High Altitude Observatory, National Center for Atmospheric Research, P.O. Box 3000, Boulder, CO 80307-3000, USA*

(Received 2007 May 31; accepted 2007 September 18)

Abstract

We observed small-scale magnetic-flux emergence in a sunspot moat region by the Solar Optical Telescope (SOT) aboard the Hinode satellite. We analyzed filtergram images observed at wavelengths of Fe 6302 Å, G band, and Ca II H. In Stokes I images of Fe 6302 Å, emerging magnetic flux was recognized as dark lanes. In the G band, they showed to be their shapes almost the same as in Stokes I images. These magnetic fluxes appeared as dark filaments in Ca II H images. Stokes V images of Fe 6302 Å showed pairs of opposite polarities at footpoints of each filament. These magnetic concentrations were identified to correspond to bright points in G band/Ca II H images. From an analysis of time-sliced diagrams, we derived the following properties of emerging flux, which are consistent with those of previous studies: (1) Two footpoints separate each other at a speed of 4.2 km s^{-1} during the initial phase of evolution, and decrease to about 1 km s^{-1} 10 minutes later. (2) Ca II H filaments appear almost simultaneously with the formation of dark lanes in Stokes I in an observational cadence of 2 minutes. (3) The lifetime of the dark lanes in the Stokes I and G band is 8 minutes, while that of Ca filament is 12 minutes. An interesting phenomena was observed, that an emerging flux tube expanded laterally in the photosphere with a speed of 3.8 km s^{-1}. A discussion on the horizontal expansion of the flux tube is given with refernce to previous simulation studies.

Key words: Sun: chromosphere — Sun: emerging flux — Sun: magnetic fields — Sun: photosphere

1. Introduction

An emerging flux region (EFR) is a young active region (AR) where magnetic flux loops emerge from underneath the photosphere (Bruzek 1969; Zirin 1972). Emerging flux often causes reconnection with a pre-existing coronal magnetic field, and is responsible for flares (Heyvaerts et al. 1977; Shibata et al. 1992a, 1992b; Shibata 1998; Shimizu et al. 2002). Strous et al. (1996) observed the separation speed of both polarities of emerging flux to be less than 1 km s^{-1} by using MDI magnetograms. They showed that dark lanes are often observed in the photosphere of EFRs. Harvey and Martin (1973) reported that the separation speeds of loop footpoints are around 4 km s^{-1} in the initial phase, and are reduced to 1 km s^{-1} in the later phase of emergence. The morphological features of emerging flux observed in Hα are dark loops and bright points near to their footpoints. A cluster of dark loops was named as an "arch filament system" (AFS) by Bruzek (1967). A single arch filament is thought to be a trace of a magnetic flux tube. The lifetime of an arch filament is 10–30 minutes, and the rise velocity is 10–15 km s^{-1} (Chou & Zirin 1988). The evolutions of emerging flux from the chromosphere to the corona were investigated by Yoshimura and Kurokawa (1999) and Shimizu et al. (2002). They observed that emerging flux appeared in soft X-ray images about several minutes after the appearance of a new arch filament in Hα images.

Shibata et al. (1989) performed two-dimensional magneto-hydrodynamic (MHD) simulations of emerging flux for the first time, which well reproduced various dynamical features of emerging flux, such as the rise motion of an arch filament and donwflow along it. Subsequently, three-dimensional simulations of emerging flux were carried out by Matsumoto and Shibata (1992) and others (Matsumoto et al. 1993; Fan 2001; Magara & Longcope 2001; Nozawa 2005). These three-dimentional simulations showed that when there is no strong magnetic twist, the emerging flux undergoes strong horizontal expansion in a direction perpendicular to emerging flux filament just after its emergence into the photosphere, which remains to be confirmed by actual observations.

Recently Pariat et al. (2004) proposed a new way of emergence from the Flare Genesis experiment observation

that emerging flux rises in the form of undulatory loops in the photosphere, which must be confirmed observationally by many samples of EFRs. In this paper, we report on the result of our analysis of an EFR observed by the Solar Optical Telescope (SOT) aboard Hinode. Thanks to multi-wavelength observations from space (Kosugi et al. 2007; Tsuneta et al. 2007; Suematsu et al. 2007; Ichimoto et al. 2007; Shimizu et al. 2007), we could follow the temporal evolution of emerging loops in the photosphere and the chromosphere. Our analysis concentrates on: (1) the morphological evolution of an EFR in and below the chromospheric layers and (2) basic morphological characters of individual emerging loops.

2. Observation and Data Reduction

2.1. Observation

Figure 1 shows an EFR that appeared in the moat region of NOAA 10930 near the disk center (E08°S05°) on 2006 December 19, observed with Hinode/SOT. The observation was made from 17:00 to 19:00 UT. During this period, many small-scale EFRs were observed at the south-west part of the region.

A multi-wavelength imaging observation was performed at three wavelengths, i.e., (1) Fe 6302 Å Stokes I and V, (2) G-band 4305 Å, and (3) Ca II H 3968.5 Å. The observational cadence was 2 minutes. The images in (1) were taken through the Narrow band Filter Imager (NFI) with a pass-band of 90 mÅ, while images in (2) and (3) were taken through the Broad band Filter Imager (BFI) with pass-bands of 0.8 Å and 0.3 Å, respectively. In our observation, the spatial resolutions were $0\farcs16$ pixel^{-1} (NFI) and $0\farcs10$ pixel^{-1} (BFI).

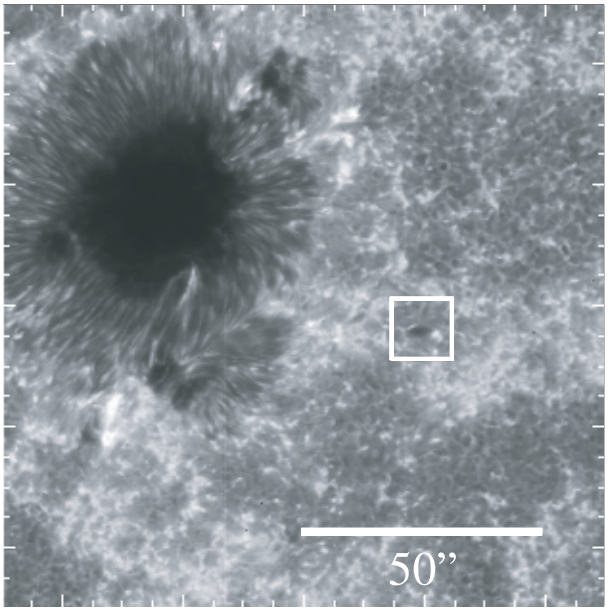

Fig. 1. Ca II H line image of NOAA 10930 obtained by Hinode/SOT at 18:01:52 UT on 2006 December 19. An EFR indicated by a white square was studied.

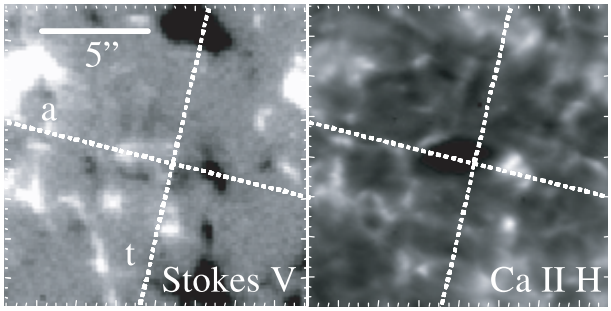

Fig. 2. Emerging flux observed in Fe 6302 Å Stokes V (left panel) and Ca II H (right panel). Two dashed lines are drawn to represent the position of two slits for time-sliced diagrams. Slit a is drawn on the two footpoints of the emerging flux (along-filament). Slit t is perpendicular to slit a, and put at the midpoint of the two footpoints (trans-filament).

2.2. Data Reduction

Co-alignment between NFI and BFI images was done with reference to common granulation patterns. To derive basic morphological properties of emerging loops, we made two kinds of time-sliced diagrams similar to those of Shimizu et al. (2002). One was an “along-filament” and the other was a “trans-filament” time-sliced diagrams, as described in figure 2.

Figures 3 and 4 show how to measure the various sizes of an emerging loop. In this study, we analyzed the evolutions of: (1) the linear size of the footpoints of an emerging loop, (2) the distance between the footpoints, and (3) the length and width of a dark lane or filament.

3. Morphological Characteristics of the EFR

3.1. Before Emergence of a Flux Tube

Figure 5 shows images of a flux tube at three stages of its emergence. The upper 4 images were taken at 17:25:51 UT, when the flux emergence had not yet occurred. Before the emerging flux’s appearance, there was no particular feature in each of the 4 images.

3.2. Initial Stage of Emergence of a Flux Tube

The middle 4 images of figure 5 were taken at 18:01:52 UT, when about 8 minutes had passed from the beginning of the flux emergence. In the image of Stokes I, there seems to be two dark lanes (1 and 2). Their widths are about $1\farcs5$ and their lengths are $4''$. There is no prominent brightening at the footpoints of the emerging flux. In the image of Stokes V, we can see a pair of opposite polarities (P_1 and N_1) at the middle of the image. They are the footpoints of the emerging flux. The distance between two footpoints is about $5''$. In the G band, we can identify two loops or filaments more clearly than in Stokes I. The widths and the lengths of the arch filaments observed in the G band are almost the same as those in Stokes I. At both ends of the arch filaments, there are tiny bright points in the G band. The size of the bright points is about $0\farcs5 \times 0\farcs5$. In the image of Ca II H, the arch filaments appear to be darker and wider. Arch filaments 1 and 2 almost

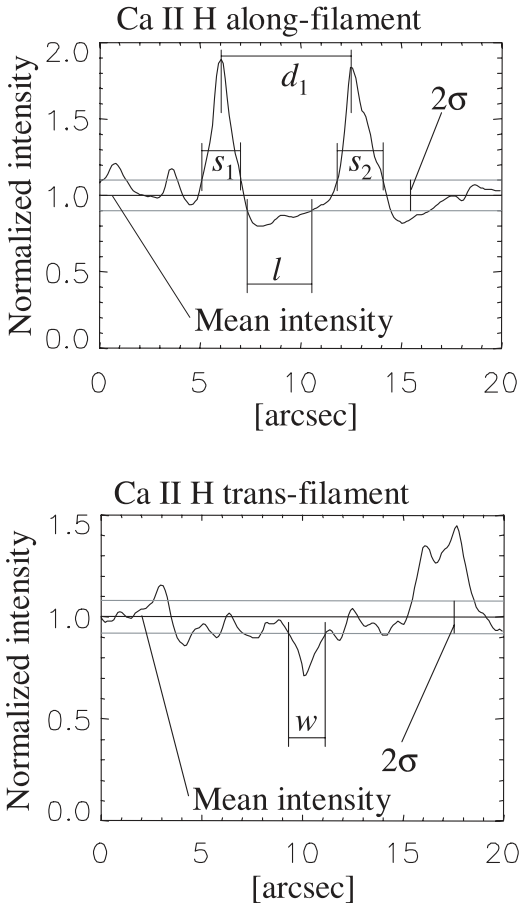

Fig. 3. Definition of linear sizes of Ca II H features. The intensity distribution was normalized by the mean intensity of the neighboring quiet region. σ is the standard deviation of the intensity fluctuation in the neighboring quiet region; d_1: is the distance between the two intensity peaks; s_1 and s_2: are the linear size of two bright points; l: is the length of the filament; and w: is the width of a dark lane/filament. The same definition is applied to Stokes I and G-band images.

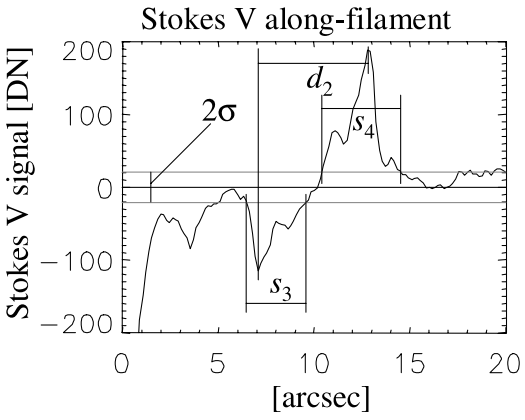

Fig. 4. Stokes V distribution on the along-filament slit. The fluctuation of the Stokes V signal on the neighborhood quiet region is expressed by σ. In the panel, d_2: is the distance between two opposite polarities of the magnetic flux; s_3 and s_4: are the linear size of the footpoints of emerging flux.

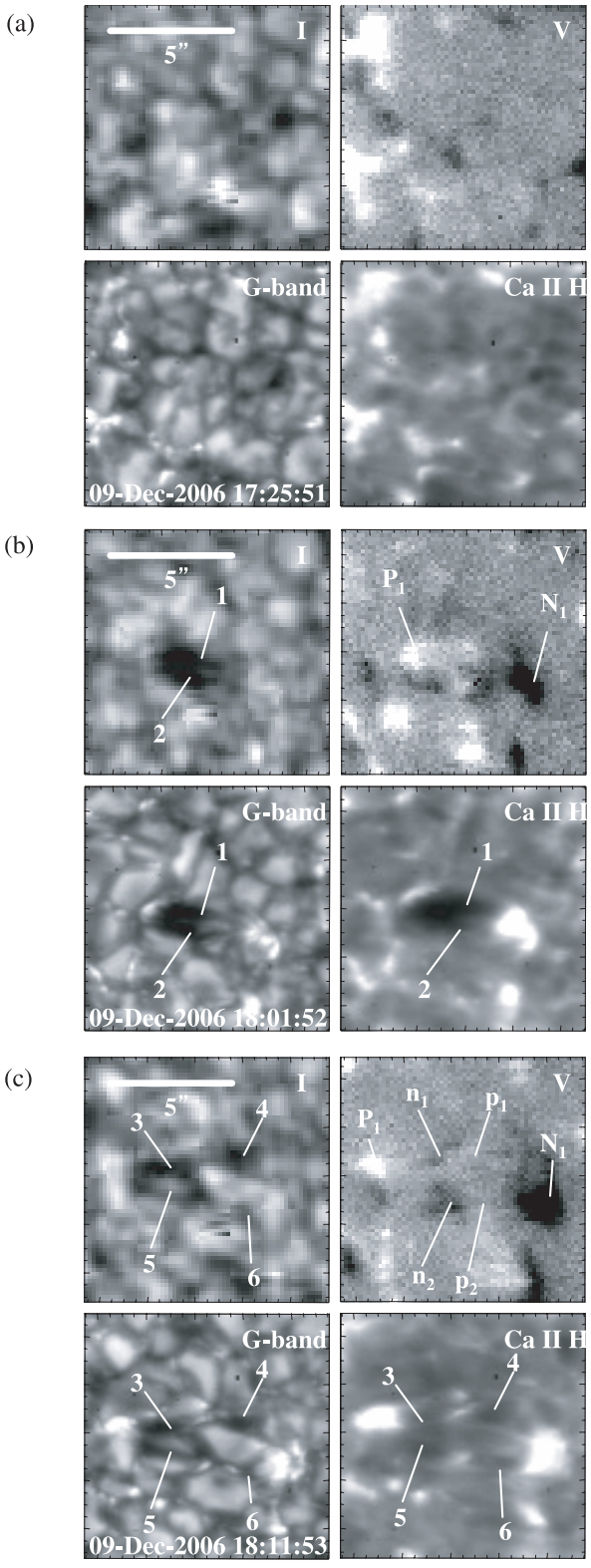

Fig. 5. Flux tube at three stages of its emergence. (a) Before emergence; (b) initial stage of emergence; (c) later stage of emergence. In each of the 4 images, upper left, upper right, lower left, and lower right show Fe 6302 Å Stokes I, V, G band, and Ca II images of the studied region with a common scale of magnification. In the images, the loops of the EFR and magnetic polarities at the loop's footpoints are indicated by numbers and letters.

merge with each other. The width of an individual arch filament is about 1″, and the whole width of the arch filaments is about 2″. The lengths of the arch filaments are about 4″, the same as in the other images.

3.3. *Later Stage of Emergence of a Flux Tube*

The bottom 4 images in figure 5 show the morphology of a flux tube at its later phase of emergence. The observation time was 18:11:53 UT, and thus 18 minutes after emergence. In the image of Stokes I we can see four dark lanes (3, 4, 5, and 6), while there are no longer any dark lanes that connect directly between the original footpoints. The widths of these dark lanes are about 0.″7 and the length of each dark lane is about 2″–3″. In the image of Stokes V, the distance between two opposite polarities is 7″, and larger than 10 minutes before. Note that in the middle region between the originally emerged footpoints there are several small magnetic concentrations (p_1, n_1, p_2, and n_2). Just as in the Stokes I image, there are four arch filaments in the G-band image. The values of the width and length of the arch filaments are also the same as those of Stokes I. The size of the bright points at the footpoints is about $1'' \times 1''$. In Ca II H image we can see four arch filaments, the same as the other images. The width of each arch filament is about 0.″5, and their length is 2″–3″. At the middle of the two main footpoints it forms new footpoints of the arch filaments. While the size of the bright points at the main footpoints is $1.''5 \times 1.''5$, that of the newly formed footpoints at the middle of the EFR is $0.''5 \times 0.''5$.

4. Temporal Evolution of an Emerging Flux Loop

In this section, we consider more quantitatively the temporal evolution of individual emerging loops.

4.1. *Evolution of the Footpoints*

Figure 6 is an "along-filament" time-sliced diagram of an emerging loop. The temporal variation of linear sizes and the mutual separation speed of footpoints measured in Stokes I and V, G band, and Ca II H are shown in figure 7.

From figure 7a, we can say that the Ca bright point is larger than that of the Stokes I/V and the G-band features. From figure 7b, the same result is obtained, except for the Stokes V feature. As can be seen in the Stokes V map in figure 6, there were pre-existing negative polarity features on the slit. Thus, the size increment of the negative polarity features after the emergence correspond to the real size of the footpoint of the emerged loop. If so, we may conclude that the size of the Ca feature is larger than those of the photospheric features in both polarities.

The footpoints of opposite polarity move away from each other at a speed of 4.2 km s^{-1} in the initial phase, and slow down to 0.8 km s^{-1} (figure 7c), which is consistent with previous work by Harvey and Martin (1973).

4.2. *Evolution of the Loops*

The along-filament time-sliced diagram of Stokes I (figure 6) clearly shows the dark lane that appeared at 17:54 UT and faded out at 18:02 UT. Thus, the lifetime was 8 minutes. The G-band time-sliced diagram shows the same behavior as that of the Stokes I. The first Ca arch filament (1 in figure 5) appeared at 17:54 UT and lasted until 18:06 UT, when at the same location two new emergences occurred (3 and 4 in figure 5). Thus, the lifetime of the Ca arch filament 1 was 12 minutes. The elongation speeds of the Stokes I dark lane, the G-band lane, and the Ca arch filament were of 2.9 km s^{-1} (figure 7d).

From the trans-filament time-sliced diagram (figure 8), we can see the evolution of the flux width. The dark lanes or filaments expanded laterally with a speed of 3.8 km s^{-1} at all wavelengths observed, and reached a width of 2.″0, although the Ca II H loop lasted longer and attained a final width of 3.″5 (figure 7e).

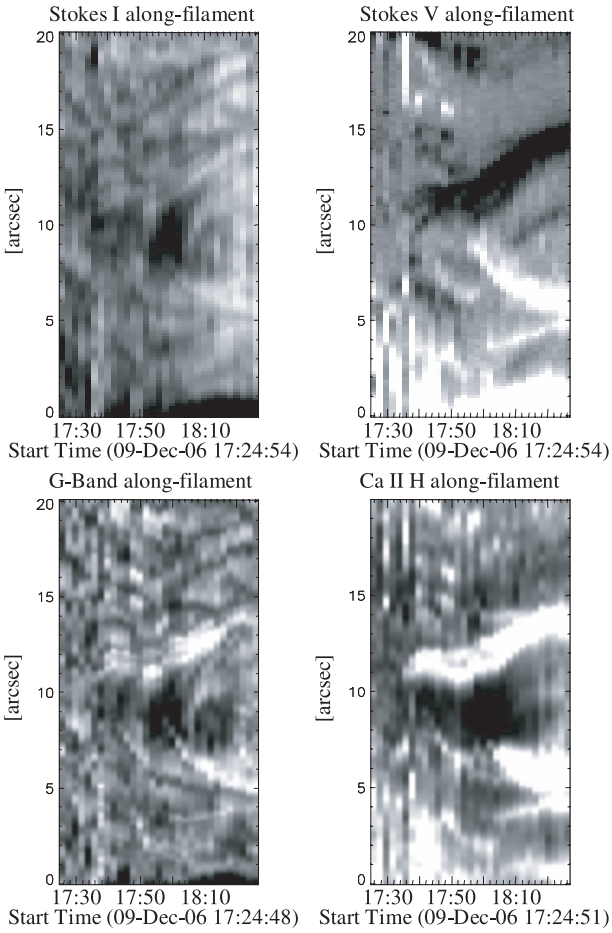

Fig. 6. Along-filament time-sliced diagram of the emerging flux. Upper left, Stokes I; upper right, Stokes V; lower left, G band; lower right, Ca II H.

5. Discussion and Summary

5.1. *Discussion*

We have confirmed that the Ca bright points in the chromosphere are larger than the features observed in the Stokes I and G band formed in the photosphere. This can be expected if the decreasing gas pressure with height allows for an expansion of the flux tube with height.

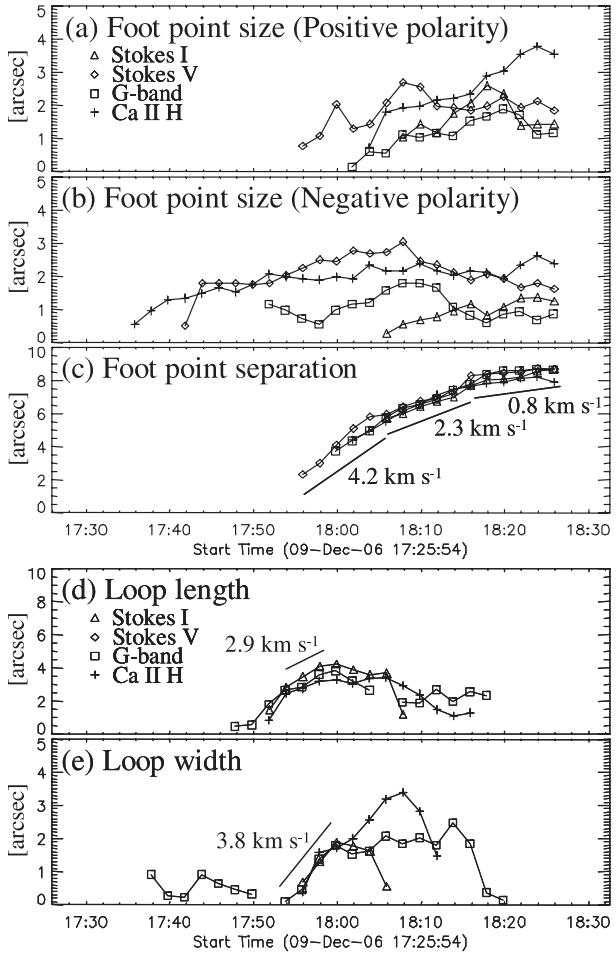

Fig. 7. Temporal evolutions of measured quantities derived from time-sliced diagrams. (a) Foot point size of positive polarities. (b) Foot point size of negative polarities. (c) Foot point separation. (d) Loop length. (e) Loop width.

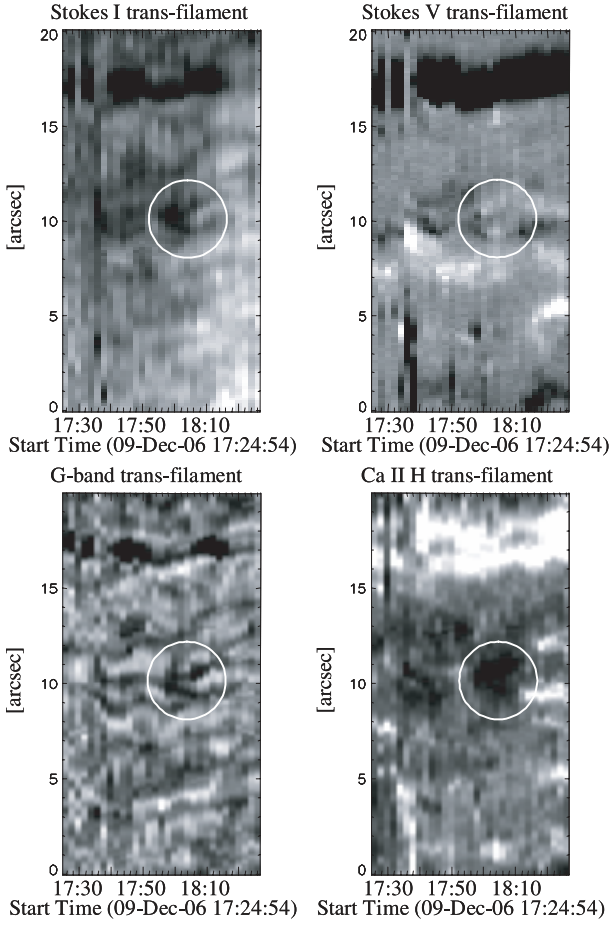

Fig. 8. Trans-filament time-sliced diagram of the emerging flux. Upper left, Stokes I; upper right, Stokes V; lower left, G band; lower right, Ca II H. Circles indicate the location of flux tube expansion.

Figure 9 shows a model of this EFR. The temporal evolution of the observed flux emergence will be as follows: (1) A magnetic flux tube emerges from the intergranular lane (17:54 UT). (2) The flux tube splits along its axis into two parts (flux tubes 1 and 2). (3) After the emergence of flux tubes 1 and 2, newly emerged flux tubes appear (flux tubes 3–6). These undulatory emergences of flux will be these observed by Pariat et al. (2004) and simulated by Isobe et al. (2007).

The horizontal expansion of an emerging flux tube in the photosphere was clearly detected in this work. What is the mechanism of flux tube expansion? This may correspond to a horizontal expansion of the emerging flux in the photosphere, theoretically predicted by three-dimensional simulations. Matsumoto et al. (1993) simulated the emergence of a non-twisted flux tube and showed that the horizontal expansion speed of flux tube is 30 km s^{-1} in the photosphere. Fan (2001) and Magara and Longcope (2001) studied the emergence of twisted flux tubes and obtained the horizontal speeds of flux tube expansion to be 6–8 km s^{-1}. Nozawa (2005) performed a comprehensive simulation of emerging magnetic flux sheets. The horizontal expansion speed of non-sheared sheets is 20 km s^{-1}, while that of sheared sheet is $\sim$10 km s^{-1}. All results of three-dimensional simulations of emerging flux tubes tell us that the horizontal expansion speed will be reduced when the tubes are twisted. As our observation showed a relatively slow speed of horizontal expansion (3.8 km s^{-1}) compared with the simulational results of non-twisted tubes expansion, the flux tube studied by us was probably a twisted one.

5.2. *Summary*

We observed an emerging flux that appeared near NOAA 10930 with Hinode/SOT. From this study, the following properties about EFRs were found:

1. The size of Ca bright points was larger than those of the Stokes I and G band.
2. Two footpoints separated from each other at a speed of 4.2 km s^{-1} during the initial phase of evolution. In a later phase, the separating rate decreased to 0.8 km s^{-1}.
3. The lifetime of the dark lanes in the Stokes I and G band was 8 minutes, while that of the Ca filament was 12 minutes.

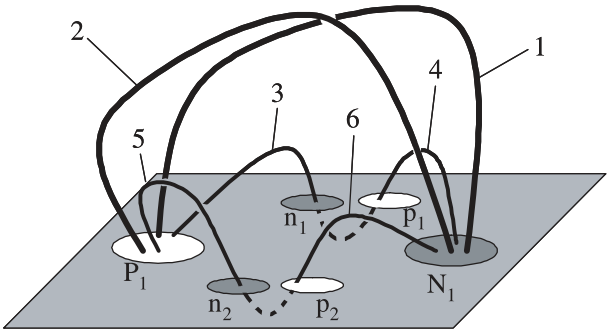

Fig. 9. Model of the EFR. White and dark ovals represent the footpoints observed with Stokes V. The solid lines stand for magnetic tubes above the photosphere and the dashed lines for those blow the photosphere. The numbers and letters in the figure correspond to the flux tubes and the footpoints in figure 5.

4. The Ca arch filament appeared within 2 minutes after the formation of the dark lane in Stokes I image.
5. The width of the Ca arch filament was 3.″5 at its maximum, wider than that of the photospheric dark lanes (2.″0).
6. The dark lanes or filaments expanded laterally with a common speed of 3.8 km s^{-1} in the photosphere and the chromosphere. The slow lateral expansion of the flux tube suggests that the flux tube was a twisted one.

The authors are partially supported by a Grant-in-Aid for the 21st Century COE 'Center for Diversity and Universality in Physics' from the Ministry of Education, Culture, Sports, Science and Technology (MEXT) of Japan, and also partially supported by a Grant-in-Aid for 'Creative Scientific Research The Basic Study of Space Weather Prediction' (17GS0208, Head Investigator: K. Shibata) from the Ministry of Education, Culture, Sports, Science and Technology. Hinode is a Japanese mission developed and launched by ISAS/JAXA, with NAOJ as domestic partner and NASA and STFC (UK) as international partners. It is operated by these agencies in co-operation with ESA and NSC (Norway).

References

Bruzek, A. 1967, Sol. Phys., 2, 451
Bruzek, A. 1969, Sol. Phys., 8, 29
Chou, D.-Y, & Zirin, H. 1988, ApJ, 333, 420
Fan, Y. 2001, ApJ, 546, 509
Harvey, K. L., & Martin, S. F. 1973, Sol. Phys., 32, 389
Heyvaerts, J., Priest, E. R., & Rust, D. M. 1977, ApJ, 216, 123
Isobe, H., Tripathi, D., & Archontis, V. 2007, ApJ, 657, L53
Ichimoto, K., et al. 2007, Sol. Phys. submitted
Kosugi, T., et al. 2007, Sol. Phys., 243, 3
Magara, T., & Longcope, D. W. 2001, ApJ, 559, L55
Matsumoto, R., & Shibata, K. 1992, PASJ, 44, 167
Matsumoto, R., Tajima, T., Shibata, K., & Kaisig, M. 1993, ApJ, 414, 357
Nozawa, S. 2005, PASJ, 57, 995
Pariat, E., Aulanier, G., Schmieder, B., Georgoulis, M. K., Rust, D. M., & Bernasconi, P. N. 2004, ApJ, 614, 1099
Shibata, K. 1998, Ap&SS, 264, 129
Shibata, K., et al. 1992a, PASJ, 44, L173
Shibata, K., Nozawa, S., & Matsumoto, R. 1992b, PASJ, 44, 265
Shibata, K., Tajima, T., Steinolfson, R. S., & Matsumoto, R. 1989, ApJ, 345, 584
Shimizu, T., et al. 2007, Sol. Phys. in press
Shimizu, T., Shine, R. A., Title, A. M., Tarbell, T. D., & Frank, Z. 2002, ApJ, 574, 1074
Strous, L. H., Scharmer, G., Tarbell, T. D., Title, A. M., & Zwaan, C. 1996, A&A, 306, 947
Suematsu, Y., et al. 2007, Sol. Phys. submitted
Tsuneta, S., et al. 2007, Sol. Phys. submitted
Yoshimura, K., & Kurokawa, H. 1999, ApJ, 517, 964
Zirin, H. 1972, Sol. Phys., 22, 34